NUMERICAL INVESTIGATIONS ON A HOT JET IN CROSS FLOW USING SCALE-RESOLVING SIMULATIONS

Benjamin M. Duda
Aerodynamic Tools & Simulations
AIRBUS Operations SAS
benjamin.duda@airbus.com

Florian R. Menter
R&D Fellow
ANSYS Germany GmbH
florian.menter@ansys.com

Marie-Josèphe Esteve
Aerodynamic Tools & Simulations
AIRBUS Operations SAS
marie-josephe.esteve@airbus.com

Thorsten Hansen
Customer Support
ANSYS Germany GmbH
thorsten.hansen@ansys.com

Sébastien Deck
Aerodynamics and Energetics Modeling
ONERA
sebastien.deck@onera.fr

Hervé Bézard
Applied Aerodynamics
ONERA
herve.bezard@onera.fr

ABSTRACT

The simulation of a jet in cross flow is of prime interest as a broad range of technical applications feature this phenomenon. However, a correct prediction still poses a challenge to modern CFD codes and turbulence models due to inherent complex dynamics and appearance of coherent structures. Jet in cross flow applications in the aeronautical area, such as auxiliary air system exhausts, additionally demand simulation strategies that allow a proper prediction of the flow field even at high Reynolds numbers. As standard statistical turbulence models show deficiencies when applied to this complex flow, a temporal and spatial resolution of turbulent scales is desired. Therefore, the applicability of Scale-Resolving Simulations (SRS) is investigated on a generic jet in cross flow configuration. Different approaches such as solving the Unsteady Reynolds-Averaged Navier-Stokes (URANS) equations as well as employing Scale-Adaptive Simulation (SAS), Delayed Detached Eddy Simulation (DDES) and Embedded Large Eddy Simulation (ELES) are validated against experimental data. Moreover, the analysis of time statistics and the transient flow field in combination with spectral analysis allow a better understanding of inherent dynamics and mixing phenomena.

INTRODUCTION AND MOTIVATION

The aerothermal design of auxiliary air system outlets is of crucial interest for the aeronautical industry in terms of reduction of weight, aircraft safety and global performance. A special challenge in this context is the simulation of a hot jet in cross flow, as it appears e.g. at discharge locations of an anti-icing system. Even though generic configurations have been investigated both experimentally and numerically, basic similarity parameters like the Reynolds number or the momentum ratio differ strongly from those which occur at aircraft related problems. The appearance and dynamics of large scale coherent structures as well as thermal mixing of jet and cross flow fluid is not yet fully understood and still a subject of debate. For a general overview on this matter, the reader is referred to the works of Margason (1993) as well as Fric and Roshko (1994).

Due to the transient and highly turbulent character of this flow, standard statistical turbulence models as well as the more elaborate Reynolds Stress Models fail in correctly predicting mean flow quantities (Acharya et al., 2001). Simulation strategies are therefore necessary that resolve at least a part of the turbulence spectrum, which will be termed Scale-Resolving Simulations (SRS). On the one hand, the use and applicability of SRS are investigated for a hot jet in cross flow and results will be compared with experimental data obtained from wind tunnel measurements carried out by ONERA and AIRBUS (Albugues, 2005). On the other hand, real time flow simulations based on scale-resolving turbulence models allow a better insight into the underlying flow dynamics and an analysis of mixing phenomena.

Similarity parameters are used to distinguish flow regimes as the establishing flow field and its dynamics can be rather different. A first important similarity parameter introduced by Callaghan and Ruggeri (1948) represents the ratio between jet and cross flow momentum and characterizes the penetration of the jet into the cross flow.

$$C_R = \frac{\rho_j U_j}{\rho_\infty U_\infty} \tag{1}$$

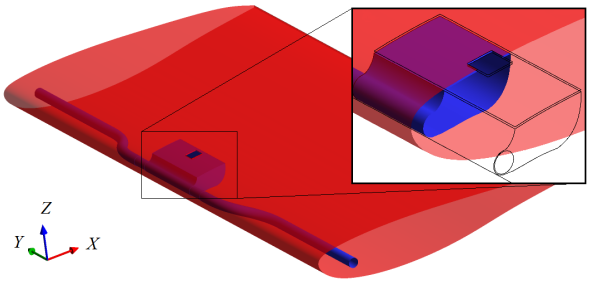

Figure 1. Generic jet in cross flow configuration

A second parameter is the cross flow Reynolds number Re_{cf}, based on a characteristic length D of the ejector, e.g. its diameter, the free stream velocity U_∞ and its kinematic viscosity ν_∞ respectively.

$$Re_{cf} = \frac{U_\infty D}{\nu_\infty} \tag{2}$$

Even though temperature differences between jet and cross flow are implicitly accounted for in Eq. (1), the absolute temperature difference $\Delta T = T_j - T_\infty$ can be used to construct a cross flow Richardson number Ri_{cf}, describing the ratio of free to forced convection with the acceleration through gravity g and the thermal expansion coefficient β.

$$Ri_{cf} = \frac{g\beta D\Delta T}{U_\infty^2} \tag{3}$$

TEST CASE DESCRIPTION

The current computational configuration corresponds to the experimental set-up investigated by Albugues (2005) and is illustrated in Fig. 1. An airfoil with 0.7m chord length and 1.4m span was designed to yield a pressure distribution representing that of a nacelle. The origin of the coordinate system is located on the symmetry plane at the downstream ejector edge on the wall, with the direction of the axes as indicated. A generic air system is integrated inside the wing and consists of two symmetrical pipes feeding hot air into a plenum. As hot air exits the plenum through a square shaped ejector with edge length $D = 30$mm, the jet in cross flow forms on the upper side of the wing. The large cross flow Reynolds number $Re_{cf} = 90\,000$ implies the broad range of appearing turbulence scales, whereas the low blowing ratio $C_R = 0.69$ is characteristic for an attached jet wake, leading to a strong thermal impact on the wall. The modest temperature difference $\Delta T = 62$K yields $Ri_{cf} \ll 1$, which means that buoyancy effects are negligible and temperature can be regarded as a passive scalar.

SIMULATION METHODOLOGY

Turbulence Modeling

As the configuration only requires a very local resolution of turbulent scales, i.e. in the jet and cross flow interaction region, simulation strategies are desired that allow the treatment of stable flow areas, such as attached boundary layers, with well established RANS capabilities. The simplest approach for SRS is therefore the solution of the URANS equations in combination with a statistical turbulence model. For this reason the $k-\omega$ Shear Stress Transport (SST) turbulence model (Menter, 1994) is employed.

The major drawback of two equation turbulence models is the fact that the turbulence scale equation (either specific dissipation rate ω or dissipation rate ε) are derived mainly from dimensional reasoning. A more rigorous starting point is the exact transport equation for kL, with L being the integral length scale of turbulence. A term-by-term modeling proposed by Menter and Egorov (2010) leads to the introduction of the von Kármán length scale L_{vK} into the transport equation. The transformation into the $k-\omega$ SST framework yields an additional source term Q_{SAS} in the ω-equation and the model was termed Scale-Adaptive Simulation (SAS).

$$Q_{SAS} = \max\left[\rho\eta_2\kappa S^2\left(\frac{L}{L_{vK}}\right)^2 - C\frac{2\rho k}{\sigma_\phi}\max\left(\frac{1}{\omega^2}\frac{\partial\omega}{\partial x_j}\frac{\partial\omega}{\partial x_j}, \frac{1}{k^2}\frac{\partial k}{\partial x_j}\frac{\partial k}{\partial x_j}\right), 0\right] \tag{4}$$

If the turbulence model is employed in a transient calculation, the von Kármán length scale allows the resolution of scales as the production of ω is increased. On the other side, capabilities of the $k-\omega$ SST model are retained in attached boundary layers.

A different approach is the Detached Eddy Simulation (DES), which is a hybrid RANS/LES formulation (Spalart, 2000). This can be achieved by blending the k-equation of the $k-\omega$ SST turbulence model with the dynamic kinetic energy subgrid-scale model for LES (Strelets, 2001).

$$\frac{\partial(\rho k)}{\partial t} + \frac{\partial(\rho U_j k)}{\partial x_j} = P_k - \rho\frac{k^{3/2}}{\min(L_t, C_{DES}\Delta)} + \frac{\partial}{\partial x_j}\left[\left(\mu + \frac{\mu_t}{\sigma_k}\right)\frac{\partial k}{\partial x_j}\right] \tag{5}$$

Consequently, in sufficiently refined areas with $C_{DES}\Delta < L_t$ the LES model is activated, whereas in coarser grid regions the $k-\omega$ SST turbulence model is employed. To avoid a switching of the models inside the boundary layer, the delayed version of this model (DDES) is used (Menter et al. 2003, Spalart et al. 2006), which forces attached boundary layers to RANS regime with the help of the $F2$ shielding function from the $k-\omega$ SST turbulence model.

The last approach considered in this context is an Embedded Large Eddy Simulation (ELES), where a spatially fixed LES region is a priori defined by the user inside the RANS domain. To avoid excessive grid refinement for wall bounded high Reynolds number flows, the Wall Modeled LES approach by Travin et al. (2006) is used. This model uses the simple Prandtl mixing length model with van Driest wall damping in the inner part of the boundary layer and switches to the Smagorinsky-Lilly model for LES in the outer part of

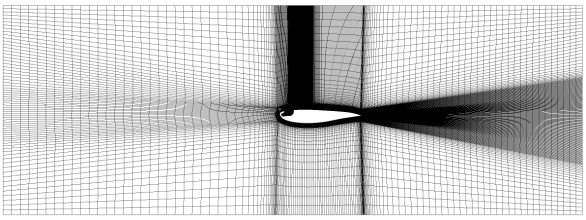

Figure 2. Computational domain with numerical grid

the boundary layer:

$$\nu_t = \min\left[(kd_w)^2, (C_{SMAG}\Delta)^2\right]\left\{1-\exp\left[-\left(\frac{y^+}{25}\right)^3\right]\right\}S \quad (6)$$

The RANS domain surrounding the ELES region is treated using the $k-\omega$ SST turbulence model. In contrast to the other approaches, where the formation of turbulent scales relies on inherent flow instabilities, fluctuations have to be prescribed at the RANS/LES interface. This is achieved with the help of the vortex method (Mathey et al., 2003), which converts modeled turbulent kinetic energy to resolved structures.

Numerical Grid and Boundary Conditions

The combination of turbulence scale resolution and heat transfer requires high quality numerical grids. For that reason a multi-block hexahedral grid with a total number of 12.9m cells was created with ANSYS ICEM CFD. In order to avoid systematical errors, the wind tunnel section around the generic jet in cross flow configuration is included in the computational domain. The minimum face angle is28.1° and the maximum cell aspect ratio 3500. A view of the grid on the symmetry plane is illustrated in Fig. 2.

All walls of the generic configuration are treated adiabatically and no slip. Integration through the viscous sublayer is necessary for heat transfer simulations, requiring a non-dimensional wall distance y^+ in the order of one. At the wind tunnel inlet a uniform velocity corresponding to $Ma_\infty = 0.138$ is defined at an ambient temperature of 291K. According to the wind tunnel characteristics, boundary conditions for turbulence quantities are specified via an eddy viscosity ratio of 10 and a turbulence intensity of 0.5%. Mass flow and temperature for the supplying pipes are prescribed corresponding to the experiment with $T_j = 353$K as well as $\dot{m} = 0.01771$kg/s for each pipe. Turbulence quantities at the pipe inlet are equal to the values of the cross flow. At the wind tunnel outlet a constant pressure boundary condition with a static pressure of 101325Pa is specified. Wind tunnel walls are treated as free slip boundaries because the influence of the developing boundary layer was found to be negligible on the wing's pressure distribution.

Numerical Scheme

All calculations were carried out using the CFD solver ANSYS FLUENT 13 with a pressure based algorithm. To reduce computational costs, a segregated solver was used, where pressure velocity coupling is achieved with the help of the SIMPLEC algorithm (Vandoormaal and Raithby, 1984). Due to different accuracy requirements, convective fluxes are discretized using a second oder upwind scheme for the URANS calculation, whereas the more accurate bounded central differencing scheme is applied for SAS, DDES and ELES. Temporal discretization is in all cases achieved by an implicit second order central difference scheme and the time step was set to $\Delta t = 5 \cdot 10^{-05}$s. Boundary layer resolution leads to high aspect ratio cells, which requires double precision for numerical accuracy. As the Mach number is small and in order to avoid pressure reflections, an incompressible ideal gas law is used, which only accounts for density changes caused by temperature differences. Considering the influence of temperature on viscosity, Sutherland's law is employed.

VALIDATION AND FLOW DYNAMICS

For turbulence model validation the procedure proposed by Sagaut and Deck (2009) is followed in which different levels of validation are defined. In the present case, three levels with increasing profoundness are investigated. These are the mean aerodynamic field, proceeding with second order time statistics, i.e. root mean square values, and concluding with one-point spectral analyses.

First and second order time statistics were collected for a total number of 7000 time steps, which corresponds to the time span as the cross flow passes 25 times over the wing. As the temperature distribution behind the ejector is of prime interest in this case, the thermal efficiency η is defined as the non-dimensional expression of the local mean temperature $\bar{T}$.

$$\eta = \frac{\bar{T} - T_\infty}{T_j - T_\infty} \quad (7)$$

This value is plotted in Fig. 3 along the symmetry line at the wall. The URANS calculation shows the least agreement in both near field and far field. Especially the strong temperature gradient $\partial T/\partial X$ in the near field highlights the poor mixing prediction capabilities of this approach. In contrast to this, SAS, DDES and ELES results agree rather well with the experimental data in the far field, but show different characteristics in the near field. DDES and ELES overestimate temperature, whereas SAS shows a slight underestimation with a very good agreement in general. Fig. 4 shows the lateral spreading of thermal efficiency at a downstream location $X/D = 8$, which drastically points out the poor mixing prediction when the URANS simulation is employed. This can be attributed to the known deficiency of a standard URANS approach to overestimate turbulent viscosity, which results in an unphysical damping of spatial and temporal fluctuations. The other approaches show a very good agreement. This points out the fact that a proper prediction of mean quantities for a jet in cross flow requires the spatial and temporal resolution of the inherent dynamics. If temperature and Y-coordinate at several downstream locations X/D are scaled with the square root of X/D, all lateral distributions collapse to a single curve, as shown in Figure 5. This highlights the constant spreading rate

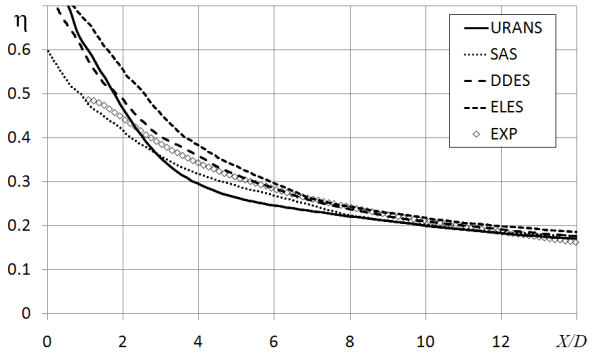

Figure 3. Thermal efficiency η along symmetry line

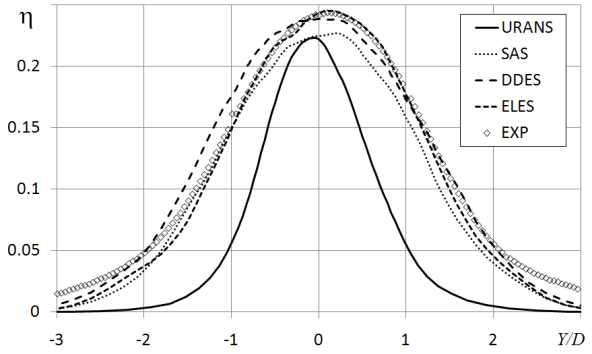

Figure 4. Lateral thermal efficiency η at $X/D = 8$

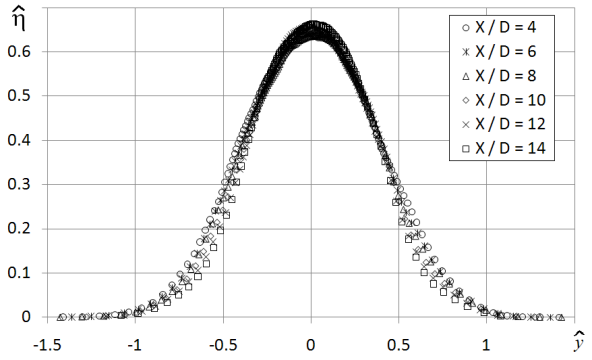

Figure 5. Self similarity lateral thermal efficiency $\hat{\eta}$

and shows the self-similarity of temperature profiles.

$$\hat{\eta} = \eta \left(\frac{X}{D} \right)^{1/2} \quad \text{and} \quad \hat{y} = \frac{Y}{D} \left(\frac{X}{D} \right)^{-1/2} \tag{8}$$

Concerning the flow topology, time averaged stream lines colored by mean temperature from SAS calculations are shown in Fig. 6. The characteristic counter-rotating vortex pair (CRVP) forms at the lateral edges of the ejector, which is usually the most dominant steady state flow feature. Due to the low momentum ratio $C_R = 0.69$, a recirculation zone of roughly $2D$ length forms behind the ejector, consisting of two

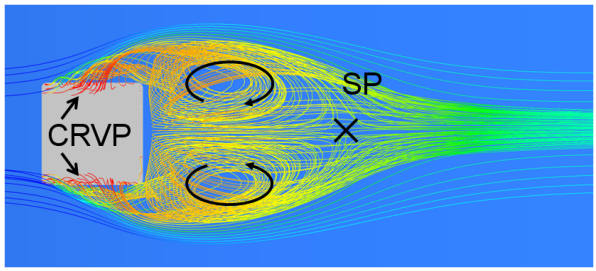

Figure 6. Stationary flow topology

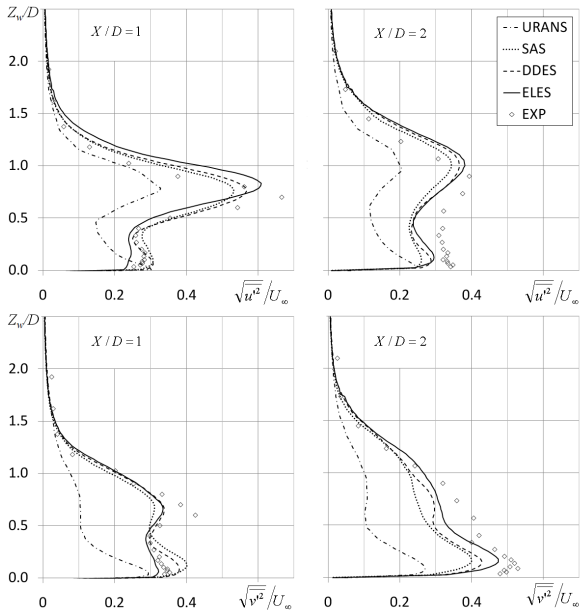

Figure 7. Second order time statistics

upright vortices. Depending on the turbulence model, strength and size of this area differ, which in turn has a strong impact on the thermal efficiency as hot air accumulates there, cf. Figure 3.

Second order time statistics are compared with experimental data for the next validation level. The profiles of the root mean square values of the X- and Y-velocity component are plotted in Fig. 7 at two different downstream locations $X/D = 1$ and 2 on the symmetry plane, with Z_w being the wall distance. For all profiles the URANS calculation shows an underestimation of the fluctuation quantities almost by a factor of two. It is interesting to notice that a qualitative agreement with the other three approaches exists, which points out that turbulent fluctuations are non-physically damped for the URANS simulation. The overall prediction quality of these quantities can be greatly increased with SAS, DDES and ELES, even if some discrepancies to experimental data remain.

The satisfying results for first and second order time statistics obtained from all SRS except URANS encourage further investigation on the transient solution behavior. For the last level of the validation process, spectral analysis is carried out for time signals sampled with a frequency of $f_s = 1/\Delta t = 20$kHz for a total of 5000 time steps. The one-sided

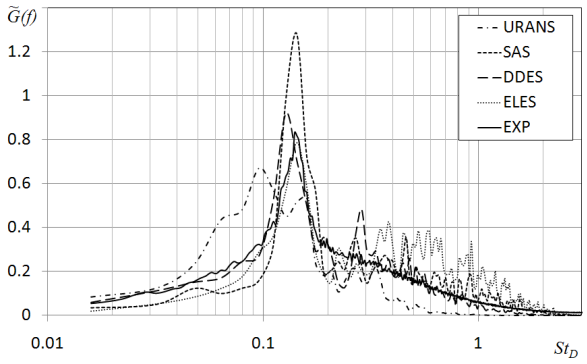

Figure 8. Spectral analysis for lateral velocity component

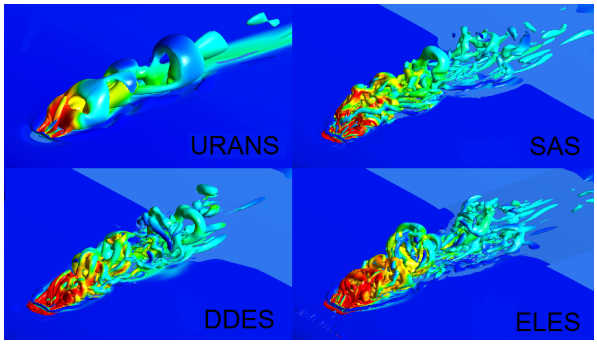

Figure 9. Transient flow topology shown by Q-criterion

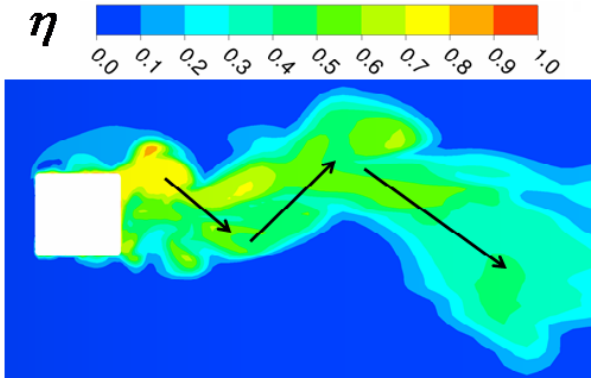

Figure 10. Instantaneous thermal efficiency η showing wake meandering at $St_D = 0.14$

power spectral density $G(f)$ was estimated using Welch's method (Welch, 1967) on 12 blocks, with 50% overlap and the Hann window function (Blackmann and Tukey, 1959). To evaluate the contribution of a frequency band to the overall fluctuation $\sigma^2 = \int G(f)\,\mathrm{d}f$, the relation $\tilde{G}_f = f \cdot G_f/\sigma^2$ is used. An example spectrum for the point $P1(D/2, 0, 2D/15)$ is illustrated in Fig. 8. Even though some dynamics are resolved for the URANS simulation, the observed peaks are less pronounced and much broader, which indicates a damped dynamical behavior for the jet. In contrast to this, the other simulations point out a strong periodic dynamic for a Strouhal number $St_D = fD/U_\infty$ around 0.14. Besides a slight underestimation for the DDES approach, this is in good agreement with the experimental data. This is also consistent with the measurements of Fric and Roshko (1994), who found a characteristic wake Strouhal number of 0.13 for a round jet, but at a higher momentum ratio of 2.

To judge the scale-resolvability, the Q-criterion (Hunt et al., 1988) is used to display turbulent structures, as illustrated in Fig. 9. The URANS calculation shows only large scale structures, whereas the other approaches allow the resolution of turbulent fluctuations. This is consistent with the spectra shown in Fig. 8, where the smaller high frequency structures are damped for the URANS simulation.

Jet Wake Meandering and Hairpin Vortices

As this characteristic frequency can be found for a number of monitor points throughout the near field of the wake, its underlying flow phenomenon and the resulting impact on thermal mixing needs further investigation. The Strouhal number is most pronounced for the lateral velocity component, which indicates a meandering of the jet wake. The origin of this flow feature can be found when looking back at the stationary flow topology illustrated in Fig. 6, as the stagnation point (SP) downstream of the recirculation zone is not fixed. Due to inherent instabilities, the stagnation point oscillates leading to an alternating flow around the recirculation zone, which consequently induces the wake meandering. This dynamical behavior differs however from the von Kármán vortex shedding for two decisive reasons. Firstly, the recirculation zone does not form a rigid obstacle for the cross flow contrary to the case of vortex shedding behind for example a rigid cylinder. Secondly, as the jet wraps around the recirculation zone, there is strictly speaking no creation of vorticity because no solid boundaries exist and consequently no shedding of vorticity. This points out the difference between the Strouhal number in the considered case and the Strouhal number observed for the von Kármán vortex shedding, $St_{vK} = 0.2$. The instantaneous surface temperature distribution in Fig. 9 clearly shows the wake meandering. The rather pronounced lateral spreading of time averaged temperature is the result of this flow phenomena. Recalling the characteristic of the URANS approach to overly damp this movement, the poor mixing prediction is explained.

Due to a strong shear layer between the cross flow and the recirculation zone, arch like vortices appear in the near field, cf. Fig. 11. They have also been observed by Andreopoulos (1984) and are characteristic for $C_R < 1$. Their decay within a distance of $3-5D$ downstream of the ejector can be attributed to the grid coarsening. Caused by the dynamics of the wake in combination with the high Reynolds number, these structures experience strong deformation. This is illustrated by the spectral analysis of the temperature signal on point $P2(2D, 0, 4D/3)$ in Fig. 12, which shows a broad band contribution in the range between $St_D = 0.4$ and $St_D = 0.6$. Depending on the turbulence model, differently pronounced spectral peaks are found with the most dominant one for the SAS turbulence model at $St_D = 0.4$. In strong contrast to this, the URANS spectrum shows a less pronounced peak at St_D around 0.2 and no high frequency components at all. This highlights once more the incapability of a standard URANS approach to resolve turbulent fluctuations. As these structures entrain cold cross flow fluid into the jet wake, they play an

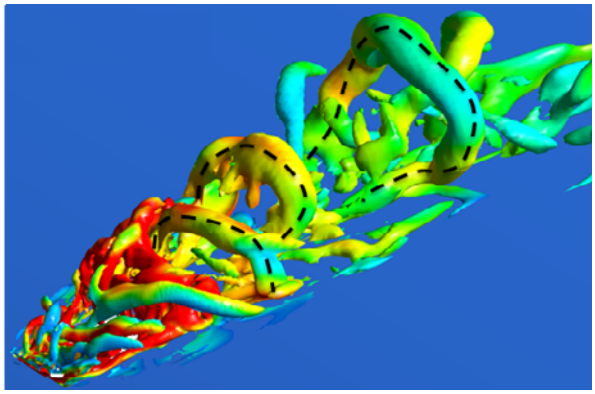

Figure 11. Hairpin vortices

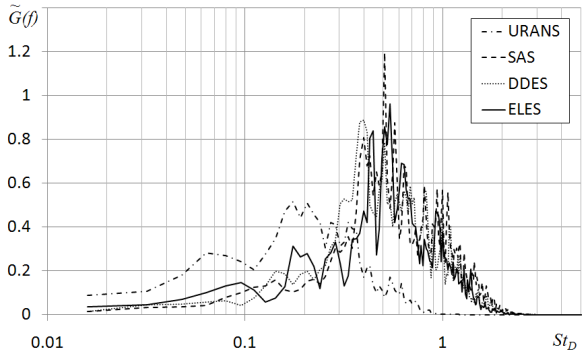

Figure 12. Spectral analysis for temperature

important role for the thermal mixing process and require resolution for a proper prediction of the temperature distribution.

CONCLUSION

Scale-Resolving Simulations have been carried out for the prediction of a hot jet in cross flow at a high Reynolds number and a low momentum ratio. URANS exhibits deficiencies in a correct prediction of the mixing process due to the strong damping of the jet wake and incapability of resolving turbulent fluctuations. In contrast to this, SAS, DDES and ELES show good agreement for first and second order time statistics with experimental data and spectral analysis confirmed a dominant frequency at $St_D = 0.14$. This dynamical behavior is attributed to a meandering of the jet wake, which is different to the von Kármán vortex shedding and explains the enlarged lateral spreading of temperature downstream of the ejector. The lateral temperature distribution at different downstream locations in the far field shows a self similarity when scaled with $\sqrt{X/D}$. Additionally, hairpin vortices, which develop in a less periodic manner around the recirculation zone, were identified with the help of the Q-criterion.

REFERENCES

Acharya, S., Tyagi, M. and Hoda, A., 2001, "Flow and heat transfer predictions for film cooling", Annals of the New York Academy of Sciences, Vol. 934, issue 1, pp. 110-125.

Albugues, L., 2005, Analyse expérimentale et numérique d'un jet débouchant dans un écoulement transverse, Ph.D. Thesis, L'Ecole Nationale Supérieure de l'Aéronautique et de l'Espace, Toulouse, France.

Andreopoulos, J., 1985, "On the structure of jets in cross-flow", J. Fluid Mech., Vol. 157, pp. 163-197.

Blackman, R. B. and Tukey, J. W., 1959, "Particular Pairs of Windows", The Measurement of Power Spectra, From the Point of View of Communications Engineering", New York: Dover, pp. 98-99.

Callaghan, E. E. and Ruggeri, R. S, 1948, "Investigation of the Penetration of an Air Jet Directed Perpendicularly to an Air Stream", Technical Note 1615, National Advisory Committee for Aeronautics.

Fric, T. F. and Roshko, A., 1994, "Vortical structure in the wake of a transverse jet", J. Fluid Mech., Vol. 279, pp. 1-47.

Hunt, J. C., Wray, A. A. and Moin, P., 1988, "Eddies, stream, and convergence zones in turbulent flows", Center for Turbulence Research Rep. CTR-88.

Margason, R. J., 1993, "Fifty years of jet in cross flow research" in Computational and Experimental Assessment of Jets in Cross Flow, Vol. CP-534, pp. 1.1-1.41.

Mathey, F., Cokljat, J. P., Bertoglio, J. P. and Sergent E., 2003, "Specification of LES Inlet Boundary Condition Using Vortex Method", Proceedings, 4th International Symposium on Turbulence, Heat and Mass Transfer.

Menter, F. R., 1994, "Two-equation eddy-viscosity turbulence models for engineering applications", AIAA Journal, 32 (8), pp. 269-289.

Menter, F. R, Kuntz, M. and Langtry R., 2003, "Ten Years of Industrial Experience with the SST Turbulence Model", Proceedings, 4th International Symposium on Turbulence, Heat and Mass Transfer.

Menter, F. R. and Egorov, Y., 2010, "The Scale-Adaptive Simulation Method for Unsteady Turbulent Flow Predictions, Part 1: Theory and Model Description", Flow, Turbulence and Combustion, Vol. 85, pp. 113-128.

Sagaut, P. and Deck, S., 2009, "Large eddy simulation for aerodynamics: status and perspectives", Phil. Trans. R. Soc. A., Vol. 367, pp. 2849-2860.

Spalart P. R., 2000, "Strategies for turbulence modelling and simulations", Intl. J. Heat Fluid Flow, Vol. 21, pp. 252-263.

Spalart, P. R., Deck, S., Shur, M. L., Squires, K. D., Strelets, M. K. and Travin, A., 2006, "A new version of detached-eddy simulation, resistant to ambiguous grid densities", Theor. Comput. Fluid Dyn., Vol. 20, pp. 181-195.

Strelets, M., 2001, "Detached Eddy Simulation of Massively Separated Flows", AIAA Journal, Vol. 2001-0879.

Travin, A. K, Shur, M. L, Spalart, P. R. and Strelets, M. K., 2006, "Improvement of Delayed Detached-Eddy Simulation for LES with Wall-Modelling", Proceedings, ECCOMAS CFD.

Vandoormaal, J. P. and Raithby, G. D. 1984, "Enhancements of the SIMPLE Method for Predicting Incompressible Fluid Flows", Numerical Heat Trsnfer, Vol. 7, pp. 147-163.

Welch, P. D., 1967, "The Use of Fast Fourier Transform for the Estimation of Power Spectra: A Method Based on Time Averaging over Short, Modified Periodograms", IEEE Transactions on Audio and Electroacoutics, Vol. Au-15, pp. 70-73.